


RESEARCH ARTICLE

A random encounter model for wildlife density estimation with vertically oriented camera traps

Shuiqing He^{1,2} , J. Marcus Rowcliffe², Hanzhe Lin^{1,3}, Chris Carbone², Yorrick Liefing¹, Shyam K. Thapa^{4,5}, Bishnu P. Shrestha^{1,6} & Patrick A. Jansen^{1,7}¹Department of Environmental Sciences, Wageningen University, Wageningen, the Netherlands²ZSL Institute of Zoology, Regent's Park, London NW1 4RY, UK³Environmental Research Center, Duke Kunshan University, Kunshan, Jiangsu, China⁴Zoological Society of London, Nepal Office, Kathmandu, Nepal⁵National Trust for Nature Conservation, Lalitpur, Nepal⁶Department of National Parks and Wildlife Conservation, Kathmandu, Nepal⁷Smithsonian Tropical Research Institute, Ancon, Panama, Republic of Panama**Keywords**

Bardia National Park, camera traps, detectability, mammal community, Nepal, photogrammetry, random encounter model

CorrespondencePatrick A. Jansen, Department of Environmental Sciences, Wageningen University, Wageningen, the Netherlands. Telephone: +31 317 48 58 28. E-mail: patrick.jansen@wur.nl**Funding Information**

This research was supported by Himalayan Tiger Foundation for funding the Bardiya survey, a Chinese Scholarship Council (CSC) to S.H. for the PhD project and the Wildlife Ecology and Conservation Group of Wageningen University and Research.

Editor: Prof. Nathalie Pettorelli**Associate Editor:** Dr. Tim Hofmeester

Received: 13 March 2024; Revised: 12 November 2024; Accepted: 15 November 2024

doi: 10.1002/rse2.427

Introduction

Animal abundance estimates are essential to answer important questions in ecology and conservation biology (Buckland et al., 2005; Gopalaswamy et al., 2012). Camera trapping has become a major method for estimating densities of terrestrial mammals (Gilbert et al., 2021; Meek

Abstract

The random encounter model (REM) estimates animal densities from camera-trap data by correcting capture rates for a set of biological variables of the animals (average group size, speed and activity level) and characteristics of camera sensors. The REM has been widely used for setups in which cameras are mounted on trees or other structures aimed parallel to the ground. Here, we modify the REM formula to accommodate an alternative field of view acquired with vertically oriented camera traps, a type of deployment used to avoid camera theft and damage. We show how the calculations can be adapted to account for a different detection zone with minor modifications. We find that the effective detection area can be close to a rectangle with dimensions influenced by the properties of the Fresnel lens of the camera's motion sensor, the body mass of different species and the height of the camera. The other REM parameters remain the same. We tested the modified REM (vREM) by applying it to wildlife data collected with vertically oriented camera traps in Bardia National Park, Nepal. We further validated that the effective detection area for the camera model used was best approximated as a rectangle shape using maximum likelihood estimation. Density estimates obtained broadly matched independent density estimates for nine species from the previous studies in Bardia with varying body sizes by four orders of magnitude. We conclude that these modifications allow the REM to be effectively used for mammal density estimation for species with a wide range of body sizes, with vertically oriented camera traps.

et al., 2019). Camera-trap surveys are economical, efficient and non-invasive, as well as providing clear and robust evidence of species occurrence (Pfeffer et al., 2018; Sanderson & Trolle, 2005). However, one of the limitations of this technique is that cameras themselves are expensive and can be vulnerable to damage or theft, which can bring great financial and data losses (Meek

et al., 2016). In sites with poachers or elephants, for example, placements close to the ground have a high risk of theft or destruction (Grassman et al., 2005; Glover-Kapfer et al., 2019).

Vertical orientation of camera traps, in which camera traps are mounted several metres above the ground facing straight down, is an effective solution to minimize the risk of damage from animals like bears or elephants and theft by humans in such situations (Grassman et al., 2005; Meek et al., 2016). Besides the reduced risk of vandalism and theft, a more clearly defined detection zone and reduced habitat disturbance have been put forward as advantages of a vertical orientation (Smith & Coulson, 2012). In addition, mounting off the ground may also make cameras less vulnerable to wildfire, especially in areas with seasonal forest fires.

One common goal of camera trapping is to estimate population densities of mammal species as to inform conservation and management. Among these, the random encounter model (REM) (Rowcliffe et al., 2008) is one of the most reliable and most often used approaches (Palencia et al., 2022; Schaus et al., 2020). REM estimates animal densities from camera-trap data by correcting capture rates for a set of biological variables of the animals (average animal group size, speed and activity level) and characteristics of camera sensors. Currently, the REM and other approaches for estimating animal density from camera traps are designed for horizontal setups (Howe et al., 2017; Rowcliffe et al., 2008). To apply the REM to vertical setups, modifications are required.

Here, we modify the standard formula of the detection zone of the REM so that it can be used for wildlife density estimation with vertical camera-trap orientations, as vREM. We show how the effective detection area must be calculated as a rectangle, depending on the properties of the lens of the camera's motion sensor. Then, we test the vREM by applying it to wildlife data collected with vertical camera traps in Bardiya National Park, Nepal, a species-rich protected area, and compare the resulting density estimates for 12 species varying in size over 4 orders of magnitude (3.713–3160 kg) with independent estimates from former studies. Our study provides broadens the application of density estimation using the REM to a novel camera placement strategy.

Methods

From horizontal to vertical

The REM was adapted from the classic two-dimensional gas model, in which the expected number of contacts is simply the ratio of area covered by all particles present to the total area (Hutchinson & Waser, 2007). Manipulating

this equation and applying it to animals and cameras allows animal density to be estimated from the capture rate (y) for a survey period (t). For horizontal setups, the effective detection area – the contact zone of animals and the camera – is a sector-shaped area, defined by radius r and angle θ , within which the camera's passive infrared motion sensor detects passing animals. The profile (\bar{p}) is calculated by the width of the covered path presented to animals by the detection zone averaged across all possible angles of approach (Rowcliffe et al., 2008). The density of an animal species with velocity v , activity level a and group size g can then be calculated (Formula 1).

$$D = \frac{y}{t} \times \frac{\pi g}{v \cdot a \cdot r(2 + \theta)} = \frac{y}{t} \times \frac{g}{va\bar{p}} \quad (1)$$

Two key components of any PIR sensor are the pyroelectric sensor and the Fresnel lens. The pyroelectric elements use the pyroelectric effect to generate an electrical current when they are at different temperatures from one another. The Fresnel lens is the optics of the PIR trigger which alters where in the environment the pyroelectric sensor is 'looking'. Fresnel lenses can be either single-zone or multi-zone, containing single or multiple detection windows composing the 'detection zone' of the camera (Welbourne et al., 2016). Based on this, different types of Fresnel lenses can have different shapes of detection zones.

Three camera-trap models were used in this project: Browning BTC-5HDPX, Reconyx HC500 (HYPERFIRE) and Reconyx HYPERFIRE 2 (Table S4). From the detection area of their PIR Fresnel lenses (Figs. S4 and S5), it seems a priori likely that the effective detection zone in vertical setups is best described by a rectangle with a detection angle of 2π radians, defined by half width and half height of the rectangle, a and b (Formula 2 and Fig. 1). Based on this assumption, through a coordinate system using the directions of a and b as the x and y axes, the approach profile of the detection zone can be calculated from the transverse line of the rectangle with the approaching direction of the animal (Formula 2). Imagine an animal approaching the detection zone from a direction γ , the profile of the detection zone from this angle of approach should be the perpendicular distance between the two lines (l_1 and l_2) that cut across the diagonal points (A & B) of the rectangle (Fig. 1). The profile can be derived from two times the distance between the origin (O) and the crosspoint (C) between l_2 and its perpendicular line (Formula 3) that goes through the origin (Formulas 4 and 5). The average profile (\bar{p}) in this model can then be calculated through trigonometry and integration (Formulas 6 and 7). The integration range of g was set between 0 and $\frac{\pi}{2}$ assuming symmetry of rectangle.

$$y = \tan\gamma(x-a) - b \quad (0 \leq a \leq b; 0 \leq \gamma \leq \pi/2) \quad (2)$$

$$y = -(1/\tan\gamma)x \quad (3)$$

$$\tan\gamma(x-a) - b = -(1/\tan\gamma)x \quad (4)$$

$$OC = \sqrt{\left(\frac{a \tan^2 \gamma + b \tan \gamma}{\sec^2 \gamma}\right)^2 + \left(-\frac{a \tan \gamma + b}{\sec^2 \gamma}\right)^2} \quad (5)$$

$$p = 2OC = 2(asin\gamma + bcos\gamma) \quad (6)$$

$$\bar{p} = \frac{\int_0^{\pi/2} 2(asin\gamma + bcos\gamma) d\gamma}{\frac{\pi}{2}} = \frac{2(a+b)}{\frac{\pi}{2}} = \frac{4(a+b)}{\pi} \quad (7)$$

Photogrammetry

The width of the field of view on the ground (d) was calculated from field of view angle (α , provided by the manufacturer, Table S4) and height of camera (h) using the following formula:

$$d = 2h \tan \frac{1}{2} \alpha \quad (8)$$

Given image width in pixels (W), and the distance of an animal from the image origin (the midpoint of the image) in pixels (w), its real-world distance from the origin can then be calculated as: $w d / W$.

Animal tracking

Movement paths were tracked by tagging pixels using the same frontmost foot consistently across all images of a

group observation (a continuous sequence of photo records of a group of animals with given species passing the camera) as the tracking point and converting to real-world position as above for estimation of parameters including detection zone and animal movement speed. Only the first individual to trigger the camera within one group observation was tracked for detection zone and speed estimation. Speeds were calculated by dividing the summed distance moved across images by time elapsed, given by the difference between timestamps of the last and first images of the observations.

Detection zone estimates

The half width and height of the rectangle detection zone (a and b in Fig. 1) were estimated by fitting detection functions (Buckland et al., 2001) to distances from the origin in the first image of each observation in, respectively, the x and y axes of the image plane. The rectangle dimensions were assumed to potentially differ between camera models, to increase with increasing body mass (Rowcliffe et al., 2011; Schmidt-Nielsen, 1984) and to increase with increasing height of the camera.

Field Test

Study site and data collection

To assess the performance of vREM applied to field scenario, we applied it to data collected in the western part

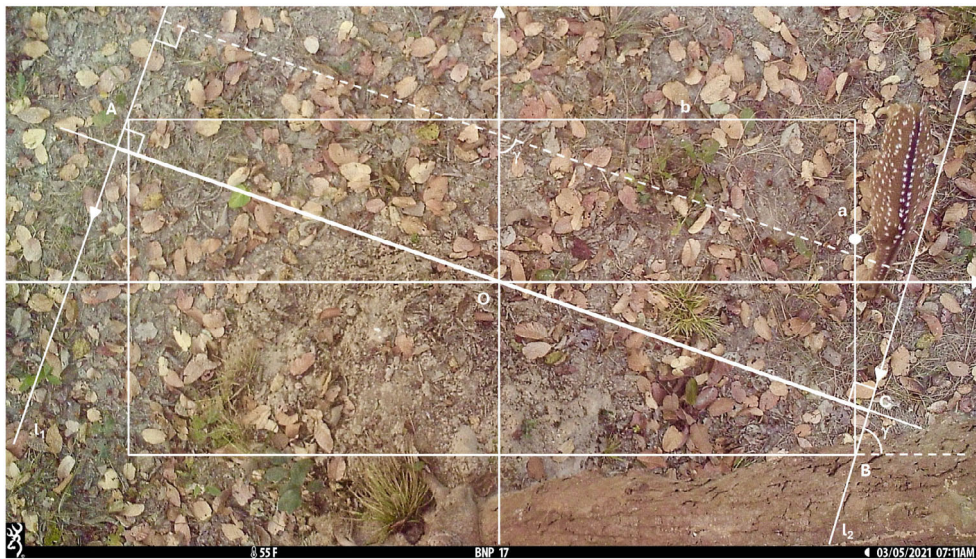


Figure 1. Diagram illustrating the profile (bold line) of a rectangle detection zone when an animal is approaching. The rectangle is defined by half the width and height, a and b . l_1 and l_2 go across the diagonal points A and B of the rectangle with orientation reflecting the direction of approach (γ) of the animal.

of Bardiya National Park (BNP), located in the Terai lowlands of southwestern Nepal. BNP covers a protected area of 968 km² and is comprised by a landscape of sal (*Shorea robusta*) forests, grasslands, mixed forests and riverine forests (Dinerstein, 1979a; van Lunenburg et al., 2017). BNP is well known as a habitat rich in bird and mammal species with a record of 513 bird species and 62 mammal species including a large range of carnivores, mesoherbivores and megaherbivores (Bardia National Park Office, 2022; DNPWC & DFSC, 2022; Kral & van Lunenburg, 2017).

The survey used a 1.4 × 1.4 km grid of 50 vertically placed camera traps with PIR triggers mounted at heights ranging from 4.5 to 8.4 m (Fig. 2). The camera traps were put on the trees by field staff with ladders or elephant-back and climbing. The heights from camera traps to the ground were measured with tape. Images of the observations were stored in Agouti, an online platform and database for processing and archiving of camera-trap images (Casaer et al., 2019). Animals in the images were identified and annotated using an AI

algorithm which have been trained for vertical camera trapping images for over four years of data, combined with manual validation and annotation. No time limit was given to a single observation. If the time gap between two subsequent observations is lower or equal to 2 min, these two observations were then merged into one. We used a dataset that covers the period between May 10, 2018 and Mar 16, 2022. Deployments with wrong time records due to failures of the internal clocks of the cameras were deleted, including deployments with a wrong starting time and ending time. The total sampling effort in the remaining dataset was 32 144 days. All data analyses and visualizations were done in R version 4.4.0 (R core Team, 2024).

vREM parameter estimates

Animal tracking

The minimum sample size for parameter estimation was set at 150 (Bollen et al., 2023; Palencia et al., 2022;

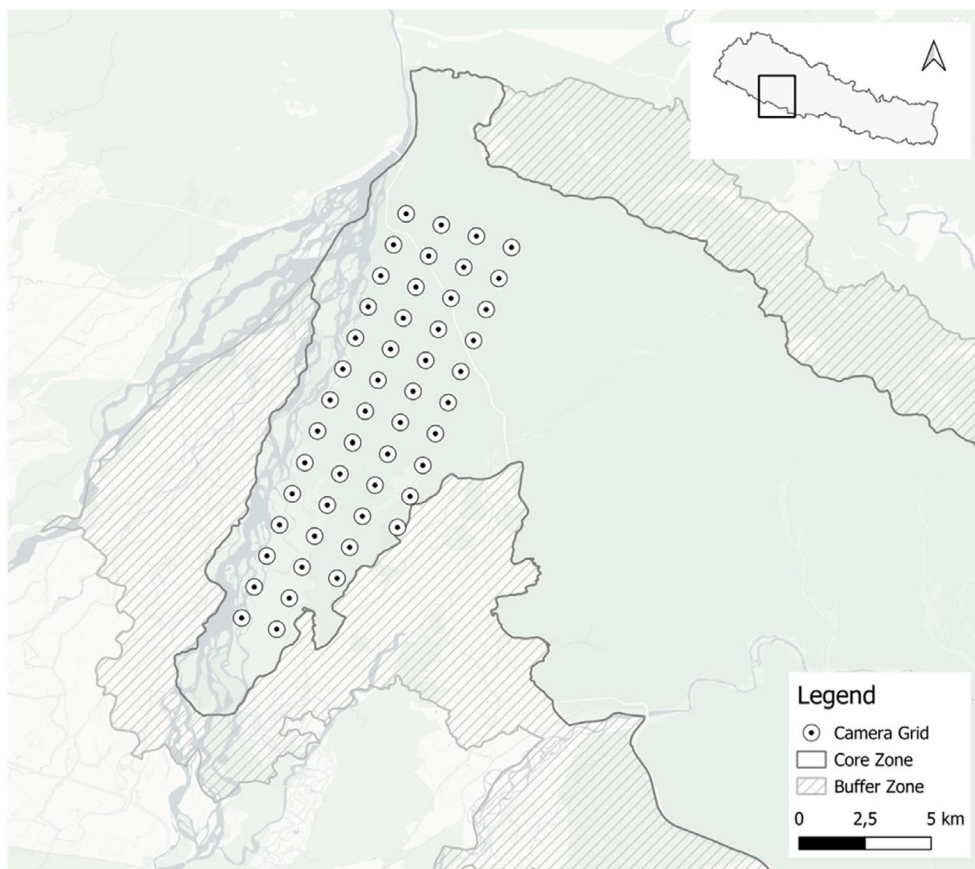


Figure 2. Map of the study area within the western part of Bardiya National Park, showing the grid camera traps used in the survey. The inset in the top right of the figure shows the location of Bardiya National Park within Nepal.

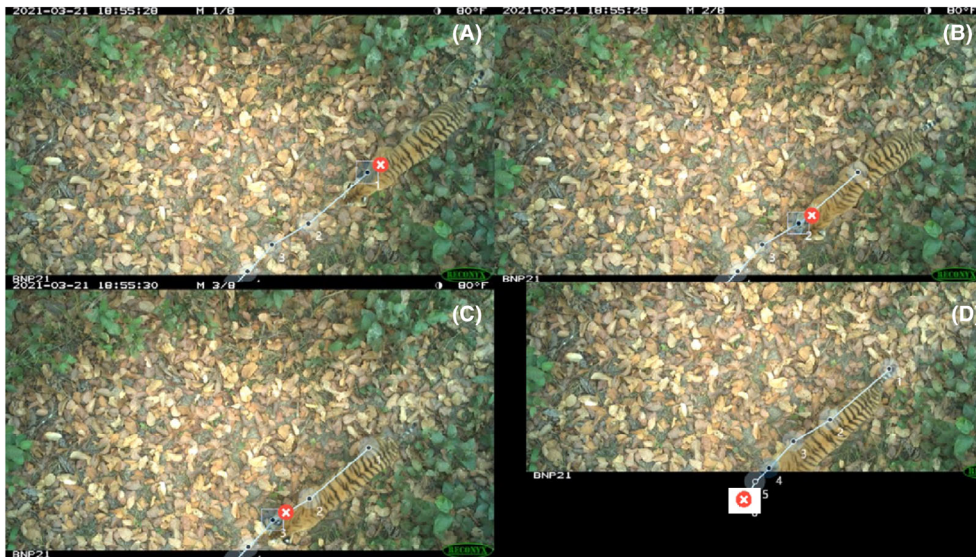


Figure 3. Animal tracking in Agouti. Images A to D show the track of a tiger passing through the detection view. Each point was consistently pinned to one of the animal's front feet (in this case the right foot). D shows the situation when the front foot was out of view and the point was therefore approximated outside the image frame.

Rowcliffe et al., 2011). To meet or exceed this target, we tracked animals in all records for species with fewer than 300 observations. For with more than 300 observations, 300 observations were randomly selected. For all but one species (golden jackal (*Canis aureus*) speed, $n = 63$), sample sizes exceeded 100, and the sample sizes of three species fell between 100 and 150 (Indian crested porcupine speed (*Hystrix indica*), $n = 104$; Nepal gray langur (*Semnopithecus schistaceus*), $n = 127$; Asian elephant, $n = 135$). The locations were also estimated and marked both inside and outside the view (Fig. 3). Similarly, if the front foot was obscured by an animal's body, the foot position was estimated. For greater one-horned rhinoceros (*Rhinoceros unicornis*) and Asian elephants (*Elephas maximus*), in contrast, the central point of the body part shown in the first photo was selected as the tracking point.

Detection zone estimates

The number of observations per species used to model the detection zone ranged from 107 (golden jackal) to 594 (chital (*Axis axis*)) (Table S1). To validate the assumption that the detection zone is a rectangle, the first-triggered points of each species were plotted separately (Fig. 4) and combined using an empirical distribution with the absolute values of x and y coordinates in metres (Fig. S2). Based on the distribution plots of the first triggers, we assumed that the distribution of the x and y axis distances followed a bivariate normal distribution in a rectangle-shaped detection zone, with the mid-point of the image as the origin of the rectangle-shaped

detection zone (Figs. 4 and S2). The height and length, which together define the sizes and shapes of the rectangles, were then estimated through the maximum likelihood function using height of the camera traps, body mass and camera types as covariates (Table 1).

Three different types of cameras were used in this study, each with a different field of view (Table S4). Image metadata included the pixel dimensions of the image, the position of the tracking points, the deployment ID, the time of the records and the information of the species.

Maximum Likelihood Estimation was applied using the *mle2* function from the *bbmle* package (Bolker, 2022). The Akaike Information Criterion (AIC) was applied to assess the best-fitting model with different covariates to get half the height and width of the rectangle detection zones through the coefficients result. The estimated profiles of different species in different camera heights and types were then calculated with the major and minor axes through integral (Formula 7). Bootstrap with 1000 resamples of the integral results of the profiles was applied to calculate the standard error with *boot* function from *boot* package (Canty & Ripley, 2022; Davison & Hinkley, 1997).

Movement speed, activity level and group size

The number of observations per species used to estimate speed varied from 63 (golden jackal) to 312 (chital). Activity level was estimated using all observations, without weighing for group size. Sample size for estimating

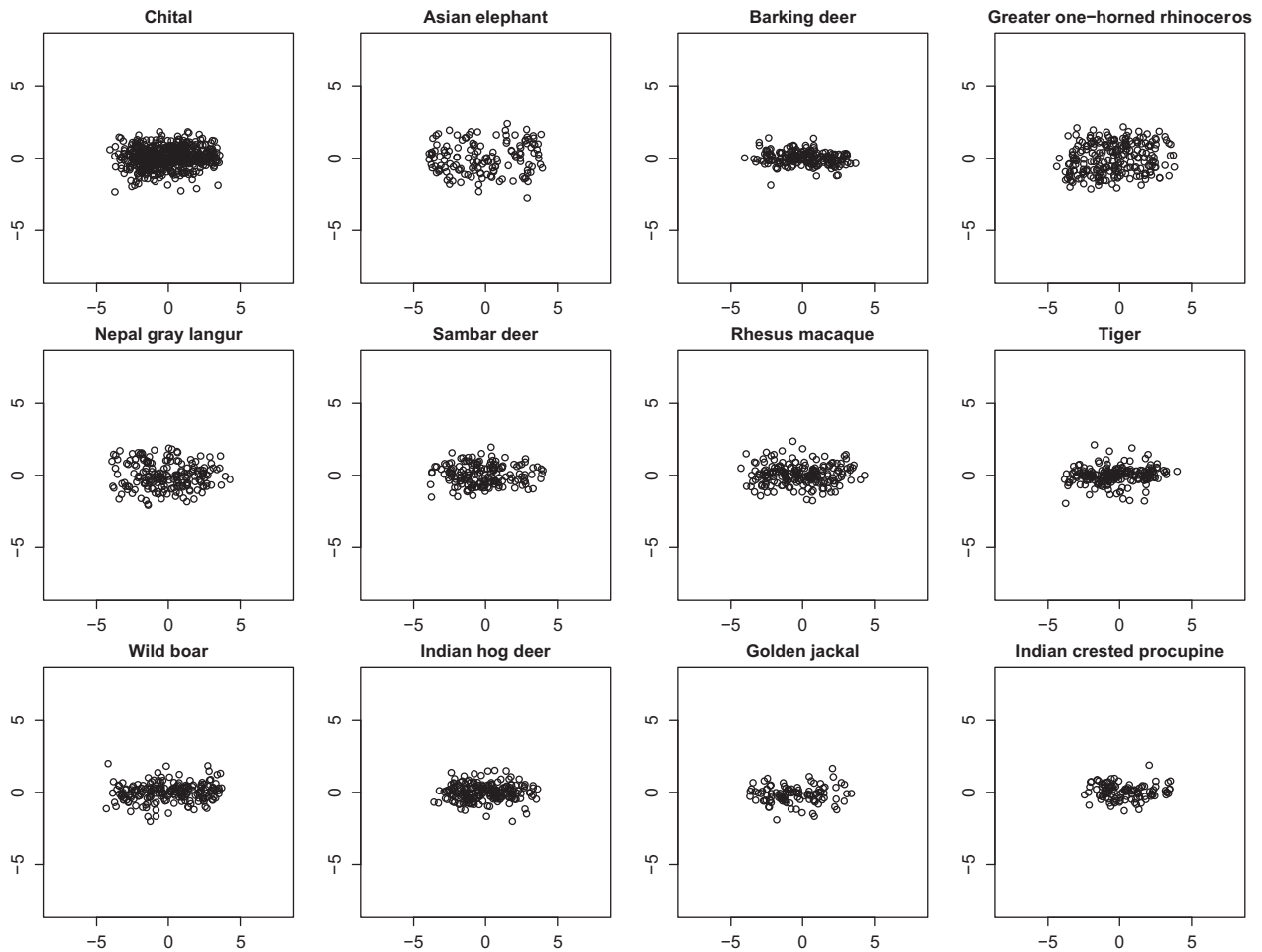


Figure 4. First trigger positions of 12 mammal species in Bardiya. The midpoints of the graphs were set as the origins. The unit of the axes is in metres.

group size ranged from 108 (golden jackal) to 22 512 (chital) (Table S1). The harmonic mean of speed observations was used to estimate the average speed (m/s) through *hmean* function from *sbd* package in R, which serves to reduce the impact of faster speeds on the mean speed since animals are more likely captured while moving faster than while moving slowly (Rowcliffe, 2022b; Rowcliffe et al., 2016). Movement paths that included periods of animal inactivity (speed < 0.01 m/s) were excluded.

To estimate the animal activity level (proportion of time spent active), we used the *fitact* function from the R package *activity*, in which a circular kernel density is fitted to radian time-of-day data to estimate the activity level from the distribution (Rowcliffe, 2022a; Rowcliffe et al., 2014). To account for variation in day length during the study, clock time was converted to the solar time before activity level estimation using *solartime* function

from *activity* package (Vazquez et al., 2019). Group size (*g*), the mean number of animals per observation, was included in the density calculation as in Formula (1) since the unit of photo rate was the group not the individual (Rowcliffe et al., 2008).

Results

Fifty-eight species were recorded in this survey, including 18 bird species, 1 amphibian species and 39 mammalian species (Table S3). The most recorded species was chital with 23 308 observations, followed by rhesus macaque (*Macaca mulatta*), Nepal gray langur and barking deer (*Muntiacus muntjak*). Together, these species encompassed 97.5% of all animal observations.

Among all estimated parameters, group size showed little variation across species (from 1.03 to 2.04). Conversely, activity level displayed slightly greater variability

Table 1. Coefficients from the summary result of the best fit model using $m/e2$ function: $0.5 \times \text{width} \sim \text{height} + \text{body mass} + \text{camera type}$; $\text{ratio} \sim \text{camera type}$. $0.5 \times \text{width}$ was ln-transformed and body mass was power-transformed with an exponent of $2/3$ (Schmidt-Nielsen, 1984).

Response	Estimate	Std. error	Z value	Pr (z)
0.5 × width intercept: Browning	-0.6156	0.1832	-3.3607	***
0.5 × width height (m):	0.1618	0.0245	6.6121	***
0.5 × width body mass (kg)	0.0020	0.0002	11.3377	***
0.5 × width intercept: Reconyx HC500	-0.9700	0.0521	-6.7980	***
0.5 × width intercept: Reconyx Hyperfire 2	-0.8760	0.0367	-7.0963	***
Ratio: Browning	0.3680	0.0084	43.7651	***
Ratio: Reconyx HC500	0.5914	0.0419	5.3297	***
Ratio: Reconyx Hyperfire 2	0.3705	0.0192	0.1335	

Note: The ratio (height/width) defines the shape of the detection zone from different types of camera traps.

*** $P < 0.001$.

(from 0.29 to 0.75). Average speed while active showed pronounced variation (from 0.09 to 0.39 m/s). The vREM estimates of species density ranged from 0.22 km^{-2} (tiger, *Panthera tigris*) to 155 km^{-2} (chital) (Table 2).

To validate the vREM density estimates, we compared them with independent density estimates for nine species, sourced from four published surveys carried out in BNP (Table S5). A Wald test on chi-square distribution with 1 degree of freedom was applied to compare the difference between the vREM estimates and reference estimates with standard errors. For rhinoceros, the actual population size was known; hence, this density estimate has no standard error. We found a broad match between vREM and independent estimates (Fig. 5 and Table 3).

Discussion

In this study, we modified the REM to a vREM to work with vertically oriented camera traps. This involved an alternative way to calculate the effective detection area, which was best described by a rectangle, as well as alternative approaches to calculate the parameters from the images through photogrammetry, and an alternative formulation of the vREM density equation. We tested the method in Bardiya National Park, Nepal on 12 mammal species varying over four orders of magnitude in body mass. We found that the density estimates obtained from our results broadly matched those from previous studies in BNP across nine species for which contemporary independent estimates were available. This suggests that the vREM can be effectively used for mammal density estimation from surveys using vertically oriented camera traps.

Looking in more detail at the comparison of density between vREM estimates and independent estimates, density was similar for three out of nine species (greater one-horned rhinoceros, barking deer, and wild boar, *Sus scrofa*), slightly overestimated for one (Asian elephant), overestimated for two species (chital and tiger) and underestimated for three species (sambar deer, *Rusa unicornis*, Rhesus macaque and Nepal gray langur) (Fig. 5 and Table 3). The camera trap capture rate of macaque and langur, which are both semi-arboreal, may be biased by missed captures when they are active in the tree canopy, which might lead to the underestimation of the density of this species. For this reason, vREM might not work for semi-arboreal species. Time gaps between the reference studies and the present research may also account for some of the discrepancies observed in the estimates.

A second important factor may be a mismatch between the regions covered by the current survey and the

Table 2. 12 mammal species in Bardiya National Park and their group size, speed (m/s), activity level and density (ind/km²) estimated with the vREM.

Common name	Body mass (kg)	Observations	Trap rate (obs/100d)	Group size	Speed (m/s)	Activity level	Density (ind/km ²)
Chital	66.17	23 308	72.51	2.04 ± 0.02	0.09 ± 0.01	0.46 ± 0.00	154.88 ± 23.92
Rhesus macaque	3.71	1927	6.00	1.74 ± 0.04	0.29 ± 0.04	0.35 ± 0.01	4.49 ± 0.90
Nepal gray langur	17.35	1,144	3.56	1.62 ± 0.05	0.15 ± 0.03	0.32 ± 0.01	6.04 ± 1.22
Barking deer	15.93	709	2.21	1.07 ± 0.01	0.17 ± 0.02	0.39 ± 0.02	1.64 ± 0.35
Wild boar	101.05	630	1.96	1.62 ± 0.06	0.17 ± 0.02	0.46 ± 0.01	1.70 ± 0.32
Sambar deer	180.34	587	1.83	1.17 ± 0.03	0.18 ± 0.02	0.46 ± 0.02	1.25 ± 0.23
Tiger	162.56	436	1.36	1.03 ± 0.01	0.39 ± 0.08	0.75 ± 0.02	0.22 ± 0.05
Indian rhinoceros	1602.33	232	0.73	1.16 ± 0.02	0.24 ± 0.03	0.39 ± 0.02	0.61 ± 0.26
Indian hog deer	34.14	246	0.77	1.10 ± 0.02	0.09 ± 0.01	0.57 ± 0.02	0.80 ± 0.18
Asian elephant	3,160	233	0.73	1.45 ± 0.09	0.31 ± 0.04	0.29 ± 0.00	0.39 ± 0.09
Indian crested porcupine	12.44	117	0.36	1.23 ± 0.04	0.31 ± 0.06	0.33 ± 0.03	0.26 ± 0.06
Golden jackal	10.35	91	0.28	1.13 ± 0.04	0.31 ± 0.08	0.51 ± 0.02	0.45 ± 0.50

Note: Body mass data were sourced from PHYLACINE 1.2 (Faurby et al., 2018).

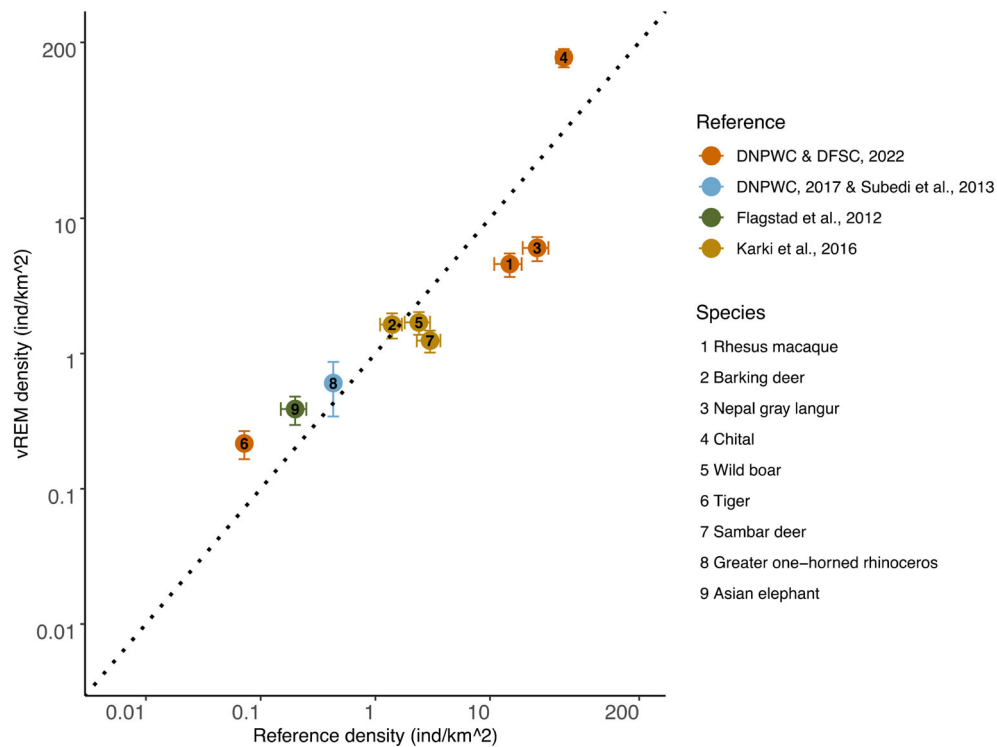


Figure 5. Comparison of density estimates from vREM (y axis) with the result of previous surveys in BNP (x axis). The black dotted line is the identity line ($y = x$). The closer the point is to this line, the more similar the results of vREM are to the previous records. Axes are logarithmic. SE bars show the uncertainty.

Table 3. Wald test result between vREM and density estimates from reference studies.

Species	W value	P value
Indian rhinoceros	–	–
Tiger	8.0507	**
Wild boar	1.0604	
Asian elephant	3.2444	
Rhesus macaque	6.2720	*
Sambar deer	5.6556	*
Barking deer	0.2676	
Chital	20.0683	***
Nepal gray langur	8.8972	**

* $p < .05$.

** $p < 0.01$.

*** $p < 0.001$.

comparisons. Our survey covered around an 80 km² section of BNP including the buffer zone lying by a perennial river, the Gerwa River, in the western part of BNP containing most of the floodplain and grassland of the whole BNP (Dinerstein, 1979a). In contrast, most comparison densities were derived from the full 968 km² park area, which is predominantly covered by sal forest. The

riverine grasslands covering much of the camera trapped region particularly attract two species, chital and tiger (Dinerstein, 1979a; Moe & Wegge, 1994; Thapa et al., 2021). Since chital is the most abundant tiger prey species, and also the possible better visibility after the fires during the hot-dry season, tigers tend to present more in grassland areas as well (Dinerstein, 1980), which can lead to overestimates of these two species. In contrast, sambar (*Rusa unicolor*) favours more continuous climax forests (Dinerstein, 1979b), which mainly occur in the eastern part of BNP outside the research area of this project. As an important help in the forest, domestic elephants were used to assist in camera deploying and checking, which can make the density of this rare species slightly overestimated.

Two species here deserve further discussion, which are rhinoceros and chital. As one of the most endangered species in Nepal, rhinoceros has been the subject of many conservation efforts over the past half a century. In BNP, since 1986, these efforts include translocation, fighting poaching, reintroduction and very close monitoring (DNPWC, 2017). For this reason, all individuals of rhinoceros within BNP are known and well monitored, while the population size of almost all other species is merely

estimated. By 2017, 35 individuals of rhinoceros lived in BNP (DNPWC, 2017). Since rhinoceros are habitat specialists, all the potential habitats of this species are within the riverine area. Therefore, the density estimate of rhinoceros from the reference is within 86 km², instead of the whole national park, which includes the Karnali floodplain, community-managed forest and Khata forest corridor (Subedi et al., 2013). This area also largely overlaps with the study area of this project.

Another species of interest is chital, the most abundant tiger prey-species in BNP with the highest density estimate from vREM. Besides the dominance and habitat selection of chital, some factors can also be responsible for a higher estimate compared with density estimation from the reference. The population of prey species, especially chital, has been increasing in recent years (DNPWC & DFSC, 2022). The widely used method of distance sampling has been applied to estimate prey density in this area for years (Buckland et al., 2001; DNPWC & DFSC, 2022). However, such a method does not perform well with thick vegetation for disturbance and low visibility (DNPWC & DFSC, 2022). For these reasons, together with personal communication with experienced field technicians who conducted the distance sampling survey, a downward bias for transect-based estimates of chital density can be reasonably expected. This, in combination with our high accuracy in estimating the reference population (i.e., rhinoceros), means that some of our relatively high-density estimates may actually be representative. Also, although the AI model in this study performs well overall, misclassifications of similar deer species occur, which may have led to an inflated chital capture rate.

A major challenge in adapting the REM to vREM was to define the best-fit shape of the effective detection area, which theoretically depends on the properties of the Fresnel lens used in PIR sensors. Based on the distribution of the 'windows' of the Fresnel lens (Welbourne et al., 2016), the shape of the distribution of the first triggered points may vary. We reasoned that the shape of the detection area should be better described as a rectangle or an oval based on the distribution of Fresnel lens of camera trap types used in this project (Figs. S4 and S5). This choice was further validated through the field test in BNP. Based on a visual examination of the distribution of the first triggers (Figs. 4 and S2), a bivariate normal distribution was observed and applied in the maximum likelihood function. A subsequent challenge was to determine the scale (ratio between width and height) and size of the detection zone based on other covariates. We found that the scale varied between camera models and that detection zone size varied significantly with species body mass and camera height as well as camera model.

One unique feature of our field application is that it yielded density estimates for 12 different species, ranging from small to megafauna, that together formed the bulk of the mammal community in a single protected area. Most REM applications to date concern one or a few species rather than entire communities (Palencia et al., 2022; Schaus et al., 2020; Wearn et al., 2022), and smaller, more cryptic species in mammal communities are often lacking in density estimates. The application in BNP explores the effective use of REM in a wider range of body sizes in a mammal community with a novel camera orientation. However, our density estimates may be less accurate estimates for species with smaller body size. The higher the camera traps go, the lower the detectability will be, especially for small and medium-sized species (Meek et al., 2016). Heights of the camera traps in this study ranged from 4.5 to 8.4 m, whereas the effective detection distance of many small- to medium-sized species in horizontal camera placements can be shorter than 4 m (Rowcliffe et al., 2011). Thus, preparatory trials to explore the proper heights of the camera trap for research species to increase the detection probability in future studies are advisable.

In conclusion, this study extends the application of REM from horizontal oriented camera traps to vertically oriented camera traps, which makes it achievable to estimate population density with vertical setups. This prospect may encourage application of vertical oriented camera traps as to protect camera traps from damage, theft and forest fire. The vREM method has the potential to contribute to the conservation and management of mammals, especially in communities where there is a diverse range of species with varying body mass.

Acknowledgements

We thank Bardiya National Park (BNP), National Trust for Nature Conservation (NTNC) and Department of National Parks and Wildlife Conservation (DNPWC) for their help and support; the Himalayan Tiger Foundation for funding the Bardiya survey, and Chinese Scholarship Council (CSC) for the PhD project; Joost de Jong and Naresh Suebdi for comments; NTNC field technicians, who diligently maintained the camera trap network in BNP, in particular Ram Raj Chaudhary, Khusiram Chaudhary, Phirulala Tharu, Tikaram Tharu, Kararu Tharu and Santigali, the elephant field technician of NTNC.

Author contributions

CC, MR, PJ, SH, and HL conceived the ideas and designed the methods; HL, MR, SH and YL built the

model and analysed the data; HL, SH, YL, ST, and BS collected the data; SH, HL, PJ, CC and MR did the writing.

Data Availability Statement

Part of the codes and related for building and verifying the model are available on github: https://github.com/Shuiqinghe/vertical_REM.

References

- Bardia National Park Office. (2022) *Management plan of Bardia National Park and its buffer zone*. Thakurdwara, Bardiya, Nepal: Nepal Ministry of Forests and Environment, Department of National Parks and Wildlife Conservations.
- Bolker, B. & R Development Core Team. (2022) *bbmle: tools for general maximum likelihood estimation*. R package version 1.0.25, <https://CRAN.R-project.org/package=bbmle>
- Bollen, M., Palencia, P., Vicente, J., Acevedo, P., Del Río, L., Neyens, T. et al. (2023) Assessing trends in population size of three unmarked species: a comparison of a multi-species N-mixture model and random encounter models. *Ecology and Evolution*, **13**, e10595. Available from: <https://doi.org/10.1002/ece3.10595>
- Buckland, S.T., Anderson, D.R., Burnham, K.P., Laake, J.L., Borchers, D.L. & Thomas, L. (2001) *Introduction to Distance Sampling: Estimating Abundance of Biological Populations*. Oxford Academic press. <https://doi.org/10.1093/oso/9780198506492.001.0001>
- Buckland, S.T., Magurran, A.E., Green, R.E. & Fewster, R.M. (2005) Monitoring change in biodiversity through composite indices. *Philosophical Transactions of the Royal Society B*, **360**, 243–254. Available from: <https://doi.org/10.1098/rstb.2004.1589>
- Canty, A. & Ripley, B.D. (2022) *boot: bootstrap R (S-plus) functions*. R package version 1.3–28.1, <https://CRAN.R-project.org/package=boot>
- Casaer, J., Milotic, T., Liefing, Y., Desmet, P. & Jansen, P. (2019) Agouti: a platform for processing and archiving of camera trap images. *BISS*, **3**, e46690. Available from: <https://doi.org/10.3897/biss.3.46690>
- Davison, A.C. & Hinkley, D.V. (1997) Bootstrap methods and their applications. *Technometrics*, **42**(2), 216–217. Available from: <https://doi.org/10.1017/CBO9780511802843>
- Dinerstein, E. (1979a) An ecological survey of the royal Karnali-Bardia wildlife reserve, Nepal. Part I: vegetation, modifying factors, and successional relationships. *Biological Conservation*, **15**, 127–150. Available from: [https://doi.org/10.1016/0006-3207\(79\)90030-2](https://doi.org/10.1016/0006-3207(79)90030-2)
- Dinerstein, E. (1979b) An ecological survey of the Royal Karnali-Bardia Wildlife Reserve, Nepal. Part II: habitat/animal interactions. *Biological Conservation*, **16**, 265–300. Available from: [https://doi.org/10.1016/0006-3207\(79\)90055-7](https://doi.org/10.1016/0006-3207(79)90055-7)
- Dinerstein, E. (1980) An ecological survey of the Royal Karnali-Bardia Wildlife Reserve, Nepal. *Biological Conservation*, **18**, 5–37. Available from: [https://doi.org/10.1016/0006-3207\(80\)90063-4](https://doi.org/10.1016/0006-3207(80)90063-4)
- DNPWC. (2017) *The greater one-horned rhinoceros conservation action plan for Nepal (2017–2021)*. Ministry of Forests and Environment, Kathmandu, Nepal: Department of National Parks and Wildlife Conservation.
- DNPWC, DFSC. (2022) *Status of tigers and prey in Nepal 2022*. Kathmandu, Nepal: Department of National Parks and Wildlife Conservation & Department of Forests and Soil Conservation. Ministry of Forests and Environment.
- Faurby, S., Davis, M., Pedersen, R.Ø., Schowanek, S.D., Antonelli, A. & Svenning, J.-C. (2018) PHYLACINE 1.2: the phylogenetic atlas of mammal macroecology. *Ecology*, **99**, 2626. Available from: <https://doi.org/10.1002/ecy.2443>
- Gilbert, N.A., Clare, J.D.J., Stenglein, J.L. & Zuckerman, B. (2021) Abundance estimation of unmarked animals based on camera-trap data. *Conservation Biology*, **35**, 88–100. Available from: <https://doi.org/10.1111/cobi.13517>
- Glover-Kapfer, P., Soto-Navarro, C.A. & Wearn, O.R. (2019) Camera-trapping version 3.0: current constraints and future priorities for development. *Remote Sensing in Ecology and Conservation*, **5**, 209–223. Available from: <https://doi.org/10.1002/rse2.106>
- Gopalaswamy, A.M., Royle, J.A., Delampady, M., Nichols, J.D., Karanth, K.U. & Macdonald, D.W. (2012) Density estimation in tiger populations: combining information for strong inference. *Ecology*, **93**, 1741–1751. Available from: <https://doi.org/10.1890/11-2110.1>
- Grassman, L.I., Tewes, M.E. & Silvy, N.J. (2005) Armoring the Camtraker® camera-trap in a tropical Asian forest. *Wildlife Society Bulletin*, **33**, 349–352. Available from: [https://doi.org/10.2193/0091-7648\(2005\)33\[349:FTFATC\]2.0.CO;2](https://doi.org/10.2193/0091-7648(2005)33[349:FTFATC]2.0.CO;2)
- Howe, E.J., Buckland, S.T., Després-Einspenner, M. & Kühl, H.S. (2017) Distance sampling with camera traps. *Methods in Ecology and Evolution*, **8**, 1558–1565. Available from: <https://doi.org/10.1111/2041-210X.12790>
- Hutchinson, J.M.C. & Waser, P.M. (2007) Use, misuse and extensions of “ideal gas” models of animal encounter. *Biological Reviews*, **82**, 335–359. Available from: <https://doi.org/10.1111/j.1469-185X.2007.00014.x>
- Kral, M.J.C. & van Lunenburg, M. (2017) The spatial distribution of ungulates and primates across the vegetation gradient in Bardiya National Park, West Nepal. *Asian Journal of Conservation Biology*, **6**, e02881. Available from: <https://doi.org/10.1016/j.gecco.2024.e02881>
- Meek, P.D., Ballard, G.A. & Falzon, G. (2016) The higher you go the less you will know: placing camera traps high to avoid theft will affect detection. *Remote Sensing in Ecology and Conservation*, **2**, 204–211. Available from: <https://doi.org/10.1002/rse2.28>
- Meek, P.D., Ballard, G.A., Sparkes, J., Robinson, M., Nesbitt, B. & Fleming, P.J.S. (2019) Camera trap theft and

- vandalism: occurrence, cost, prevention and implications for wildlife research and management. *Remote Sensing in Ecology and Conservation*, **5**, 160–168. Available from: <https://doi.org/10.1002/rse2.96>
- Moe, S.R. & Wegge, P. (1994) Spacing behaviour and habitat use of axis deer (*Axis axis*) in lowland Nepal. *Canadian Journal of Zoology*, **72**, 1735–1744. Available from: <https://doi.org/10.1139/z94-234>
- Palencia, P., Barroso, P., Vicente, J., Hofmeester, T.R., Ferreres, J. & Acevedo, P. (2022) Random encounter model is a reliable method for estimating population density of multiple species using camera traps. *Remote Sensing in Ecology and Conservation*, **8**, 670–682. Available from: <https://doi.org/10.1002/rse2.269>
- Pfeffer, S.E., Spitzer, R., Allen, A.M., Hofmeester, T.R., Ericsson, G., Widemo, F. et al. (2018) Pictures or pellets? Comparing camera trapping and dung counts as methods for estimating population densities of ungulates. *Remote Sensing in Ecology and Conservation*, **4**, 173–183. Available from: <https://doi.org/10.1002/rse2.67>
- R Core Team. (2024) *R: a language and environment for statistical computing*. Vienna, Austria: R Foundation for Statistical Computing. Available from: <https://www.R-project.org/>
- Rowcliffe, J., Carbone, C., Jansen, P.A., Kays, R. & Kranstauber, B. (2011) Quantifying the sensitivity of camera traps: an adapted distance sampling approach: quantifying camera trap sensitivity. *Methods in Ecology and Evolution*, **2**, 464–476. Available from: <https://doi.org/10.1111/j.2041-210X.2011.00094.x>
- Rowcliffe, J.M. (2022a) R package ‘activity’ [R]. <https://github.com/MarcusRowcliffe/activity>
- Rowcliffe, J.M. (2022b) R package ‘sbd’ [R]. <https://github.com/MarcusRowcliffe/sbd>
- Rowcliffe, J.M., Field, J., Turvey, S.T. & Carbone, C. (2008) Estimating animal density using camera traps without the need for individual recognition. *Journal of Applied Ecology*, **45**, 1228–1236. Available from: <https://doi.org/10.1111/j.1365-2664.2008.01473.x>
- Rowcliffe, J.M., Jansen, P.A., Kays, R., Kranstauber, B. & Carbone, C. (2016) Wildlife speed cameras: measuring animal travel speed and day range using camera traps. *Remote Sensing in Ecology and Conservation*, **2**, 84–94. Available from: <https://doi.org/10.1002/rse2.17>
- Rowcliffe, J.M., Kays, R., Kranstauber, B., Carbone, C. & Jansen, P.A. (2014) Quantifying levels of animal activity using camera trap data. *Methods in Ecology and Evolution*, **5**, 1170–1179. Available from: <https://doi.org/10.1111/2041-210X.12278>
- Sanderson, J.G. & Trolle, M. (2005) Monitoring elusive mammals. *American Scientist*, **93**, 148–155. Available from: <https://api.semanticscholar.org/CorpusID:121760640>
- Schmidt-Nielsen, K. (1984) *Scaling. Why is Animal Size so Important?* London: Cambridge University Press.
- Schau, J., Uzal, A., Gentle, L.K., Baker, P.J., Bearman-Brown, L., Bullion, S. et al. (2020) Application of the random encounter model in citizen science projects to monitor animal densities. *Remote Sensing in Ecology and Conservation*, **6**, 514–528. Available from: <https://doi.org/10.1002/rse2.153>
- Smith, J.K. & Coulson, G. (2012) A comparison of vertical and horizontal camera trap orientations for detection of potoroos and bandicoots. *Australian Mammalogy*, **34**, 196. Available from: <https://doi.org/10.1071/AM11034>
- Subedi, N., Jnawali, S.R., Dhakal, M. & Pradhan, N.M.B. (2013) Population status, structure and distribution of the greater one-horned rhinoceros *Rhinoceros unicornis* in Nepal. *Oryx*, **47**(3), 352–360. Available from: <https://api.semanticscholar.org/CorpusID:208008947>
- Thapa, S.K., De Jong, J.F., Subedi, N., Hof, A.R., Corradini, G., Basnet, S. et al. (2021) Forage quality in grazing lawns and tall grasslands in the subtropical region of Nepal and implications for wild herbivores. *Global Ecology and Conservation*, **30**, e01747. Available from: <https://doi.org/10.1016/j.gecco.2021.e01747>
- van Lunenburg, M., Kral, M.J.C. & Van Alphen, J.J.M. (2017) Decreased ungulate density in Bardiya National Park, West Nepal, and the implications for increasing tiger populations. A comment on Thapa et al. (2015). *Ethology Ecology & Evolution*, **29**, 304–309. Available from: <https://doi.org/10.1080/03949370.2016.1145147>
- Vazquez, C., Rowcliffe, J.M., Spoelstra, K. & Jansen, P.A. (2019) Comparing diel activity patterns of wildlife across latitudes and seasons: time transformations using day length. *Methods in Ecology and Evolution*, **10**, 2057–2066. Available from: <https://doi.org/10.1111/2041-210X.13290>
- Wearn, O.R., Bell, T.E.M., Bolitho, A., Durrant, J., Haysom, J.K., Nijhawan, S. et al. (2022) Estimating animal density for a community of species using information obtained only from camera-traps. *Methods in Ecology and Evolution*, **13**, 2248–2261. Available from: <https://doi.org/10.1111/2041-210X.13930>
- Welbourne, D.J., Claridge, A.W., Paull, D.J. & Lambert, A. (2016) How do passive infrared triggered camera traps operate and why does it matter? Breaking down common misconceptions. *Remote Sensing in Ecology and Conservation*, **2**, 77–83. Available from: <https://doi.org/10.1002/rse2.20>

Supporting Information

Additional supporting information may be found online in the Supporting Information section at the end of the article.

Figure S1. Diagram illustrating the profile (bold line) of an oval detection zone when an animal is approaching. The oval is defined by major and minor axes a and b . l_1 and l_2 are tangents to the detection zone parallel to each

other with orientation reflecting the direction of approach (γ) of the animal (left). Diagram illustrating the profile (bold line) of a rectangle detection zone when an animal is approaching. The rectangle is defined by half the width and height, a and b . l_1 and l_2 go across the diagonal points A and B of the rectangle with orientation reflecting the direction of approach (γ) of the animal (right).

Figure S2. Empirical distribution of the first triggered points of 16 species using the absolute values of x and y coordinates in meters. The given values represent the proportion of observations.

Figure S3. Estimated half the width (m) (y axis) distribution of species with different body mass (kg) (x axis). x

axis was power-transformed with an exponent of $2/3$ and y axis was ln-transformed.

Figure S4. Detection area of PIR in Reconyx Hiperfire (left) and Hyperfire 2 (right) from instruction manual.

Figure S5. Fresnel lens of PIR in Browning BTC-5HDPX from technical support of Browning.

Table S1. Sample size for parameter estimation.

Table S2. Comparison between vREM results in oval and rectangle shapes.

Table S3. List of all captured species.

Table S4. Camera types used in the survey.

Table S5. Previous density estimates of some mammal species in Bardiya.